NASA Technical Paper 1707

Fracture Toughness of Boron/Aluminum Laminates With Various Proportions of 0° and ±45° Plies

C. C. Poe, Jr., and J. A. Sova

NOVEMBER 1980

NASA

NASA Technical Paper 1707

Fracture Toughness of Boron/Aluminum Laminates With Various Proportions of 0° and ±45° Plies

C. C. Poe, Jr.
Langley Research Center
Hampton, Virginia

J. A. Sova
The George Washington University
Joint Institute for Advancement of Flight Sciences
Langley Research Center
Hampton, Virginia

National Aeronautics
and Space Administration

**Scientific and Technical
Information Branch**

1980

SUMMARY

The fracture toughness of boron/aluminum composites was measured on sheet specimens containing central slits of various lengths that represented cracks. The specimens were loaded axially and had various widths. The sheets tested had five laminate orientations: $[0]_{6T}$, $[0_2/\pm45]_S$, $[\pm45/0_2]_S$, $[0/\pm45]_S$, and $[\pm45]_{2S}$. Fracture toughness was calculated for each laminate orientation. Radiographs revealed that specimens began failing at the ends of the slit. Tensile failure of fibers in the principal load-carrying laminae appeared to be the cause of these failures.

A general fracture-toughness parameter Q_c, which is independent of laminate orientation, was derived on the basis of fiber failure in the principal load-carrying laminae. The value of Q_c was proportional to the critical value of the stress-intensity factor. The constant of proportionality depended only on the elastic constants of the laminates. The values of Q_c for the laminate orientations were approximately equal except for the $[0]_{6T}$ specimens with long slits and the $[\pm45]_{2S}$ specimens with small slits. The $[0]_{6T}$ specimen had too much matrix damage and the $[\pm45]_{2S}$ specimen had too much gross yielding. From published data for several other fibrous composite materials, Q_c was shown to be proportional to the ultimate tensile strain of the fibers. The fracture toughness could then be predicted solely from the ultimate tensile strength of the laminate.

INTRODUCTION

Fibrous composite materials have high specific strength and stiffness. Moreover, composite laminates can be tailored to have maximum strength and stiffness in the direction of maximum stress. Consequently composite materials have great potential for use in making minimum-weight structures. Under tension, however, most advanced composite materials are severely weakened by notches or by fiber damage. To design damage-tolerant structures, the fracture toughness of a wide range of laminate orientations must be known. Thus, a method is needed to predict fracture toughness to avoid having to test all possible laminate orientations.

Two methods were reported in references 1 and 2 for predicting the fracture toughness of graphite/epoxy (Gr/Ep) laminates from lamina properties. Each method was confirmed for only one or two laminate orientations. Three-point-bend specimens were tested. The method of reference 1 predicted the critical strain-energy-release rate G_Q as the thickness-weighted average of G_Q for the constituent laminae. The other method (ref. 2) predicted the critical stress-intensity factor K_Q for "first-ply" failure based on K_Q values for [0] and [90] laminates (i.e., fiber failure and matrix failure, respectively).

Waszczak (ref. 3) attempted to use the thickness-weighted-average method to predict K_Q for $[0/\pm45]_S$ boron/aluminum (B/Al) laminates. Both three-point-bend specimens and centrally cracked sheet specimens were tested. In this case, the predicted values were significantly larger than the measured values, especially for the centrally cracked sheet specimens. (Waszczak erroneously used elastic constants in the direction normal to the fibers for constants parallel to the fibers, and vice versa, in his calculations. Nevertheless, when the K_Q values were recalculated using the correct constants, the K_Q values were only slightly lower.) Matrix cracking parallel to the fibers at the ends of the machined slits was thought to have made K_Q for the [0] laminates artificially high and, consequently, the predictions too large. The nonlinear stress-strain behavior of the $[0/\pm45]_S$ specimens probably also contributed significantly to the discrepancy.

In the present investigation, a method somewhat like that in reference 2 was developed to predict the fracture toughness of B/Al laminates. First, the fracture toughnesses of five $[0_i/\pm45_j]_S$ B/Al laminate orientations were determined by testing axially loaded sheet specimens. The specimens had various widths and contained central, crack-like slits of various lengths. The laminate orientations were $[0]_{6T}$, $[0_2/\pm45]_S$, $[\pm45/0_2]_S$, $[0/\pm45]_S$, and $[\pm45]_{2S}$. (The stress-strain behavior of these laminates was reported in ref. 4.) The experiments indicated that failure of the principal load-carrying laminae was critical. Thus, a general fracture-toughness parameter, which is independent of laminate orientation, was derived on the basis of fiber failure in the principal load-carrying laminae. The parameter is proportional to the stress-intensity factor. (The stresses ahead of the crack tip were determined in terms of the stress-intensity factor.) The constant of proportionality depends only on the elastic constants of the laminates. Thus, once the general fracture-toughness parameter is evaluated from tests of one laminate orientation, it can be used to predict the fracture toughness (critical value of the stress-intensity factor) of other laminate orientations. The B/Al test data verified that the general fracture-toughness parameter is reasonably independent of laminate orientation, at least for those orientations investigated. Also, experimental data for several composite materials with epoxy matrices indicates that the general fracture-toughness parameter is proportional to the tensile failure strain of the fibers. When this is so, the fracture toughness of a particular laminate can then be predicted simply from the unnotched tensile strength.

SYMBOLS

a	half-length of slit, m
d	fiber spacing, m
E	Young's modulus, Pa
E_{uy}	ultimate secant modulus in y-direction, Pa
F_{tu}	material ultimate tensile strength (uncracked specimens), Pa
G	shear modulus, Pa

G_Q	critical strain-energy-release rate, J/m^2
K	stress-intensity factor, $Pa\sqrt{m}$
K_Q	critical stress-intensity factor, $Pa\sqrt{m}$
K_{Qe}	elastic critical stress-intensity factor, $Pa\sqrt{m}$
K_ε	strain-intensity factor, $\sqrt{m}$
$K_{\varepsilon Q}$	critical strain-intensity factor, $\sqrt{m}$
$K_{\varepsilon Qe}$	elastic critical strain-intensity factor, $\sqrt{m}$
L	overall specimen length, m
L_g	distance between central slit and grip, m
L_{sg}	distance between central slit and strain gage, m
Q_c	general fracture-toughness parameter, $\sqrt{m}$
r,θ	polar coordinates
S	gross laminate stress, Pa
S_c	stress at failure (strength) of cracked specimens
$[T]$	tensor transformation matrix
W	width of specimen, m
α	fiber orientation angle, deg
$[\beta]$	matrix of constitutive properties
γ	shear strain
ε	axial strain
ε_o	far-field (remote) strain
ε_{tu}	material ultimate tensile strain (uncracked specimens)
ν	Poisson's ratio
ξ_1,ξ_2,ξ_{12}	material constants given by equation (18)
ρ,ρ_ε	damage-zone sizes calculated from stress and strain, respectively, m
σ	axial stress, Pa

τ shear stress, Pa

Subscripts:

c failure

i,j ith or jth lamina

x,y Cartesian coordinates

1,2 principal lamina coordinates

FRACTURE-TOUGHNESS MEASUREMENTS

Material and Specimens

The B/Al laminates were made by diffusion bonding 0.142-mm-diameter boron fibers and 6061 aluminum foil. The laminates were used in the "as fabricated" condition, that is, they were not heat treated. The laminate orientations were $[0]_{6T}$, $[0_2/\pm45]_S$, $[\pm45/0_2]_S$, $[0/\pm45]_S$, and $[\pm45]_{2S}$. The volume fractions were 50 percent for the $[0]_{6T}$ laminate and 45 percent for the cross-plied laminates. Fracture and tensile specimens were cut from each sheet of material. The tensile specimens were tested to measure tensile stress-strain behavior for unnotched laminates. Results are reported in reference 4 and average tensile properties are included in table I for convenience. Results are also given in table I for two wider $[\pm45]_{2S}$ specimens that indicate a significant width effect. No appreciable width effect was found for the other laminate orientations.

The fracture specimens were 19.1, 50.8, and 101.6 mm wide. Crack-like slits were machined at the center of each fracture specimen with an electrical-discharge process. The width of the slits ranged from 0.18 mm to 0.25 mm. The following table lists the slit lengths for each specimen width:

Slit lengths, 2a, mm, for W of -		
19.1 mm	50.8 mm	101.6 mm
0.5	2.5	5.1
1.3	5.1	10.2
---	15.2	30.5
---	25.4	50.8

Figure 1 shows a sketch of the fracture specimen that identifies fiber angles and the locations of the strain gages and grips. The specimen length between grips was at least twice the specimen width. Also shown are a detail of the slit and a table of specimen dimensions.

Test Procedure and Equipment

The specimens were tested in a hydraulically actuated, closed-loop, servo-controlled testing machine. The load, which was measured by a conventional load cell, was used for the feedback signal. The loads were programmed by an analog ramp generator to vary linearly with time. The specimens were loaded to failure slowly (in about 2 min) so that at least 50 recordings of strain and load could be made with the data-acquisition system. (This system is described in ref. 4.)

Radiographs were made at numerous load levels during some tests of 50.8-mm- and 101.6-mm-wide specimens with $2a/W = 0.3$. The loading was held constant while each radiograph was made. The radiographs were made at various percentages of the estimated failing load, for example, 40, 60, 70, 80, and 85 percent and generally in additional increments of 5 percent until failure. The radiographs were made with an industrial-type "soft" X-ray machine with a 0.25-mm-thick beryllium window and a tungsten target. The voltage and current were set for 50 kV and 20 mA, respectively. The window of the X-ray tube was located 300 mm from the specimen, and a high-resolution photographic plate was mounted directly on the opposite side of the specimen. The exposure time for each radiograph was 12 min.

A special bracket was attached to some of the specimens to hold a gage for measuring crack-opening displacement (COD) and to minimize out-of-plane deformations that would adversely affect the COD measurements. There was no evidence that the out-of-plane deformations were large enough to significantly affect the strengths of the specimens without the bracket.

Results and Discussion

Matrix damage.- Photographs of failed 101.6-mm-wide $[0]_{6T}$ specimens with slits of different lengths are shown in figure 2. The appearance of these specimens is typical of all $[0]_{6T}$ specimens tested. All of the failed $[0]_{6T}$ specimens contained matrix cracks parallel to the fibers like those shown. The cracks were found at the ends of the slits, where shear strains are very high (refs. 5 and 6), and sometimes along the fracture path away from the slit ends. The latter type of crack probably developed sometime after the fracture initiated. The cracks at the slit ends were generally longer for shorter slits, but the cracks never extended to the ends of the specimens.

The matrix cracks were not observed before the specimens failed, even though several $[0]_{6T}$ specimens were examined and X-rayed numerous times. However, the X-rayed specimens were not observed closely between the last radiograph and failure. Thus, the cracks could have occurred close to the time of failure without notice. Therefore, one additional $[0]_{6T}$ specimen was tested and observed continuously to determine if the matrix cracks occurred before failure. That specimen was 101.6 mm wide and had a 50.8-mm-long slit. Cracks did begin to form at the slit ends, but only after the load exceeded about 93 percent of the failing load. The cracks were very small until failure.

The shear-lag analysis in reference 5 for unidirectional composites also indicates that matrix cracks at the slit ends could not have initiated much

before the time of failure. The reason is that once cracks initiated, the analysis indicates that only a small increase in load (depending on the degree of matrix ductility and the slit length) would have propagated the cracks to the ends of the specimens. Since the cracks never extended to the ends of the specimens, the cracks must have formed close to failure.

One aspect of the matrix cracking was somewhat puzzling. The shear-lag analysis in reference 5 suggests that the fractures should have initiated at the tips of the matrix cracks where the fiber stress was greatest, not almost directly ahead of the slits as shown in figure 2. Therefore, the matrix cracks must have been small or nonexistent when the fracture initiated. The cracks must have developed afterward, perhaps due to some dynamic influence of the fracture itself. The very slight noncollinearity of the slits and the fracture paths in figure 2 indicates that the fractures did initiate at the tips of very small matrix cracks like those observed in the special test noted previously. The longer and more numerous matrix cracks in specimens with short slits are perhaps further evidence of dynamic effects. Because strengths were larger for specimens with shorter slits, more energy was released during fracture.

Tirosh (ref. 6) showed that, for unidirectional laminates, the matrix yielded at the slit ends in long, narrow regions parallel to the fibers. The length of these yielded regions was proportional to the slit length and the square of the applied stress. In some of the $[0]_{6T}$ specimens, the strain gage readings indicated that the yielded regions extended quite a way toward the ends of the specimens. Figure 3 shows the applied stress plotted against the measured strain for 101.6-mm-wide $[0]_{6T}$ specimens with several slit lengths. The strain gages were located 89 mm from the slits to measure the far-field (remote) strain. (See fig. 1.) The average stress-strain curve from reference 4 is shown for comparison. Differences between the measured strains and the average stress-strain curve indicate that the yielded region extended far enough toward the strain gages to disturb the far-field strains. The data show that, for 30.5-mm- and 50.8-mm-long slits, the strains were strongly affected by the yielded regions. Near failure they even began to decrease with increasing applied stress, perhaps an effect of the matrix cracking noted previously. However, for the shorter slits, the yielded regions did not extend far enough to affect the measured strains. The measured far-field strains for 50.8-mm-wide specimens with $2a \geq 15.2$ mm were similarly affected by matrix damage. Thus, slit length and applied stress had a strong effect on the extent of the yielded regions, as Tirosh predicted.

Figure 4 shows photographs of failed specimens with the same width and slit length but with various proportions of $\pm 45^{\circ}$ laminae. The appearance of these specimens is typical. The fracture paths often began with an angle of about 38° to the slit but tended to meander. They were very inconsistent, even among duplicated tests. There was no evidence that the matrix cracked or that the measured far-field strains were affected by matrix yielding at the slit ends, even for the longest slits. Thus, the $\pm 45^{\circ}$ laminae must have provided a fairly stiff shear path to transfer load among the cut and intact 0° fibers at the slit ends, reducing the shear stresses and the extent of the yielded regions.

Fiber damage.- Figure 5 shows two radiographs of a 50.8-mm-wide $[\pm 45/0_2]_S$ laminate with a 15.2-mm-long slit. The radiographs, which show the region

around one end of the slit, were taken at 81 and 97 percent of the failing load. The circles show locations of breaks in 0° fibers. (Others have also noted 0° fiber damage in B/Al, e.g., ref. 3.) The radiographs indicate that few fibers broke before 81 percent of the failing load, whereas at 97 percent, all of the 0° fibers had apparently broken ahead of the slit end for a distance of 1.1 mm, or about six fiber spacings. (Fiber spacing was about 0.18 mm.) No broken $\pm45^\circ$ fibers were seen in the radiographs.

The photograph to the far right in figure 5 shows broken fibers near a slit end in an acutal 0° laminae of a different specimen. This $[\pm45/0_2]_S$ specimen had a longer slit and had been loaded to 95 percent of its estimated failing load. The overlaying $\pm45^\circ$ laminae were removed by leaching the aluminum matrix with NaOH. No broken $\pm45^\circ$ fibers were noticed. Thus, the interpretation of the radiographs was confirmed. The type of 0° fiber damage shown in figure 5 was typical for all laminate orientations regardless of the proportion of 0° laminae.

Broken $\pm45^\circ$ fibers were only seen in radiographs of $[0/\pm45]_S$ and $[\pm45]_{2S}$ specimens. In $[0/\pm45]_S$ specimens the number of broken $\pm45^\circ$ fibers was very small in comparison to the number of broken 0° fibers. In $[\pm45]_{2S}$ specimens, however, the number of broken $\pm45^\circ$ fibers ahead of the slit ends was as large as the number of broken 0° fibers in the other laminate orientations. Initially, the $\pm45^\circ$ fibers did not break directly ahead of the slit as the 0° fibers did. Instead, they broke along the direction of $\pm45^\circ$ fibers for a very short distance. Even so, the fracture paths were largely self-similar (collinear), as in the other laminate orientations. (See fig. 4) Therefore, the complete fracture was preceded primarily by failure of 0° fibers in all specimens with 0° fibers and by failure of $\pm45^\circ$ fibers in $[\pm45]_{2S}$ specimens.

The insert in figure 6 shows how the region of broken 0° fibers extended ahead of the slit end with applied stress for all of the laminate orientations with 0° laminae. The extent of the broken 0° fibers ρ was measured and averaged for both slit ends from radiographs like those in figure 5. For convenience the applied stress and the extent of breaks are normalized by dividing by failing stress and fiber spacing, respectively, and plotted on log-log scales. In this way the curves for different slit lengths and laminate orientations coalesced. The slopes of the curves are generally between 0.075 and 0.169, much smaller than than the 0.500 slope for a square-root singularity. Therefore, the extent of broken 0° fibers increased much faster with applied stress than linear elastic theory suggests. The slopes of the curves for $[0]_{6T}$ specimens in figure 6 are consistently larger than those for the laminate orientations with $\pm45^\circ$ laminae. This difference in slopes is probably related to the extensive matrix yielding at the slit ends in $[0]_{6T}$ specimens.

Fracture-toughness calculations.- Fracture toughness is expressed as both a stress-intensity and a strain-intensity factor. For a centrally cracked anisotropic sheet of infinite width with crack length $2a$ and applied stress S, the stress-intensity factor is $K = S\sqrt{\pi a}$, the same as for an isotropic sheet (ref. 7). A correction factor was applied to this expression to account for the finite width of the B/Al specimens. The correction factor was calculated with the finite-element computer program in reference 8 and the elastic constants in table I. The resulting values for all the B/Al laminate orientations were

virtually identical to those for isotropic sheets. Therefore, the stress-intensity factor for the finite-width B/Al specimens was written as

$$K = S\sqrt{\pi a \sec (\pi a/W)} \tag{1}$$

where W is the specimen width and $\sqrt{\sec (\pi a/W)}$ is a widely used expression for the isotropic finite-width correction factor. To account for fiber damage at the slit ends and to give finite strength for $2a = 0$, the damage-zone size ρ was added to the slit length so that equation (1) becomes

$$K = S\sqrt{\pi (a + \rho) \sec (\pi a/W)} \tag{2}$$

The value ρ was not included in the finite-width correction term because ρ was assumed to be much smaller than W, so

$$\sec [\pi (a + \rho)/W] \approx \sec (\pi a/W)$$

At failure, equation (2) gives the critical stress-intensity factor

$$K_Q = S_c\sqrt{\pi (a + \rho_c) \sec (\pi a/W)} \tag{3}$$

where S_c is the strength and ρ_c is the size of the damage zone at failure. When there is no slit ($2a = 0$), the strength S_c in equation (3) equals the material ultimate tensile strength F_{tu}. Thus, ρ_c and K_Q are related by

$$\rho_c = \frac{\left(K_Q/F_{tu}\right)^2}{\pi} \tag{4}$$

By eliminating ρ_c from equation (3) with equation (4) and solving for K_Q,

$$K_Q = \frac{K_{Qe}}{\sqrt{1 - K_{Qe}^2/\left(\pi a F_{tu}^2\right)}} \tag{5}$$

where

$$K_{Qe} = S_c\sqrt{\pi a \sec (\pi a/W)} \tag{6}$$

is the elastic critical stress-intensity factor. For long slits, $K_Q \approx K_{Qe}$.

The stress-strain behavior of the B/Al laminates was very nonlinear (ref. 4). The degree of nonlinearity increased with the proportion of $\pm 45^\circ$ laminae. For laminates with 0° laminae, however, strains were "controlled" by the relatively linear 0° laminae. It was thought that the effect of a nonlinear compliance could largely be avoided by analyzing the data in terms of strain rather than stress. Therefore, the data were also analyzed with a strain-intensity factor defined as

$$K_\varepsilon = \varepsilon_o\sqrt{\pi(a + \rho_\varepsilon) \sec (\pi a/W)} \tag{7}$$

where ε_o is the remote strain in the loading direction and ρ_ε is the damage-zone size for strain. By following the same procedure used to derive equation (5),

$$K_{\varepsilon Q} = \frac{K_{\varepsilon Qe}}{\sqrt{1 - K_{\varepsilon Qe}^2/(\pi a \varepsilon_{tu}^2)}} \tag{8}$$

where $K_{\varepsilon Q}$ is the critical strain-intensity factor, ε_{tu} is the material ultimate tensile strain, and

$$K_{\varepsilon Qe} = \varepsilon_{oc}\sqrt{\pi a \sec (\pi a/W)} \tag{9}$$

is the elastic critical strain-intensity factor where ε_{oc} is the remote strain at failure. Similar to equation (4), the size of the damage-zone size at failure is

$$\rho_{\varepsilon c} = \frac{(K_{\varepsilon Q}/\varepsilon_{tu})^2}{\pi} \tag{10}$$

For a linear elastic material with uniaxial loading, $\varepsilon_{oc} = S_c/E_y$ and $\varepsilon_{tu} = F_{tu}/E_y$. Consequently,

$$K_{\varepsilon Q} = K_Q/E_y \tag{11}$$

and

$$\rho_{\varepsilon c} = \rho_c$$

The K_Q and $K_{\varepsilon Q}$ values were calculated with equations (5) and (8), respectively, for each specimen. They are listed in table II along with the values for gross stress and remote strain at failure. When strain gage instrumentation failed, remote failing strains were calculated from the failing stresses with the Ramberg-Osgood equations in reference 4. Calculated strains were also used in lieu of measured strains for $[0]_{6T}$ specimens with $2a \geq 15.2$ mm. As shown previously, these measured strains did not accurately represent remote strains. (Both calculated and measured strains are given in table II(a).) The K_Q and $K_{\varepsilon Q}$ calculations were made with the average tensile properties in table I. The different values of F_{tu} and ε_{tu} in table I for $[\pm 45]_{2S}$ specimens of different widths were used to calculate K_Q and $K_{\varepsilon Q}$ for fracture specimens of corresponding widths.

Average values of K_Q and $K_{\varepsilon Q}$ and the respective coefficients of variation for these values are given in table III for each laminate orientation. The K_Q values increased with the proportion of 0° laminae, much like the ultimate tensile strengths in table I. On the other hand, except for the $[\pm 45]_{2S}$ specimens, the $K_{\varepsilon Q}$ values are approximately equal. They are similar to the ultimate tensile strains in table I, which were limited by failure of the 0° laminae. For the $[\pm 45]_{2S}$ specimens, the average $K_{\varepsilon Q}$ value is elevated due to very large values for specimens with small slits. These specimens yielded overall and had very large failing strains. (See table II(e).) For $[0_2/\pm 45]_S$ and $[\pm 45/0_2]_S$ specimens, the K_Q and $K_{\varepsilon Q}$ values are approximately equal, whereas the ultimate tensile strengths and strains are noticeably different. Thus, stacking sequence affected F_{tu} and ε_{tu} values but not K_Q and $K_{\varepsilon Q}$ values.

The coefficients of variation in table III are relatively small for laminate orientations with both 0° and $\pm 45^\circ$ laminae. However, values are fairly large for $[0]_{6T}$ and $[\pm 45]_{2S}$ specimens, especially the latter. For $[0]_{6T}$ specimens, the large coefficient of variation is probably due mainly to the extensive matrix damage at the ends of the slits. When the extent of damage is large compared with slit length, the stress-intensity factor analysis is not necessarily valid. The strain gage readings gave clear evidence that the extent of damage was large for $[0]_{6T}$ specimens with $2a \geq 15.2$ mm. In fact, the stress-intensity factor analysis may not have been very accurate for the other $[0]_{6T}$ specimens because the K_Q and $K_{\varepsilon Q}$ values in table II(a) increased somewhat with slit length over the entire range of lengths.

For $[\pm 45]_{2S}$ specimens, the coefficient of variation is large for several reasons. First, scatter is large among results in table II(e) for duplicate specimens. The difference between results for those specimens that were X-rayed and those that were not suggests that a viscoelastic effect is present. Also,

the width effect manifested in the unnotched tensile properties is present in the results for specimens with slits, at least for small slits. The coefficient of variation is much larger for $K_{\varepsilon Q}$ than K_Q because failing strains (and consequently $K_{\varepsilon Q}$ values) are very large for small slits. (For the other laminate orientations, the coefficients of variation are about the same for $K_{\varepsilon Q}$ and K_Q.)

Table III also contains values of ρ_c and $\rho_{\varepsilon c}$ that were calculated with equations (4) and (10) using the average values of K_Q and $K_{\varepsilon Q}$. (For $[\pm 45]_{2S}$, values were calculated for each specimen width.) The difference between ρ_c and $\rho_{\varepsilon c}$, which is due to the nonlinear stress-strain behavior, is small for $[0]_{6T}$ and increases with the proportion of $\pm 45^\circ$ laminae as expected. However, except for $[\pm 45]_{2S}$ specimens, the difference between ρ_c and $\rho_{\varepsilon c}$ is not very great. The values of damage-zone size in table III agree well with the measured values shown in figure 6. They are also similar to those reported elsewhere for graphite/epoxy composites (e.g., ref. 9). Some investigators have speculated that damage-zone size at failure is independent of laminate orientation, but there is some evidence in table III and figure 6 that damage-zone size increases somewhat with the proportion of $\pm 45^\circ$ laminae.

FRACTURE-TOUGHNESS PREDICTIONS

A General Fracture-Toughness Parameter

For the laminate orientations with both 0° and $\pm 45^\circ$ laminae, the 0° laminae carried more of the applied load than the $\pm 45^\circ$ laminae could carry alone. If the 0° laminae failed, the $\pm 45^\circ$ laminae would be overloaded. Therefore, failure of the 0° laminae would be critical for all the laminate orientations investigated here except for $[\pm 45]_{2S}$, for which failure of the $\pm 45^\circ$ laminae would obviously be critical. These critical laminae will hereinafter be referred to as the principal load-carrying laminae. Unnotched ultimate tensile strengths for those laminate orientations with both 0° and $\pm 45^\circ$ laminae were predicted quite well in reference 4 with this criterion.

For specimens with slits, the experimental results discussed previously showed that complete fracture was preceded by tensile failure of the fibers ahead of the slits in the principal load-carrying laminae. Strains for these fibers can be derived from the solution in reference 7 for singular stresses in an anisotropic, homogeneous sheet containing a through-the-thickness crack. The sheet was assumed to be in a state of plane stress. For a specially orthotropic material with Mode I loading, the singular stresses just ahead of the crack tip ($\theta = 0$ in fig. 7) simplify to

$$\begin{Bmatrix} \sigma_x \\ \sigma_y \\ \tau_{xy} \end{Bmatrix} = \frac{K}{E_y\sqrt{2\pi r}} \begin{Bmatrix} \sqrt{E_x E_y} \\ E_y \\ 0 \end{Bmatrix} \tag{12}$$

where K is the stress-intensity factor. The shear stress τ_{xy} is zero because of symmetry. The strains are thus given by

$$\begin{Bmatrix} \varepsilon_x \\ \varepsilon_y \\ \gamma_{xy} \end{Bmatrix} = \frac{K[\beta]}{E_y\sqrt{2\pi r}} \begin{Bmatrix} \sqrt{E_x E_y} \\ E_y \\ 0 \end{Bmatrix} \tag{13}$$

where $[\beta]$ is the matrix of constitutive properties:

$$[\beta] = \begin{bmatrix} 1/E_x & -\nu_{yx}/E_y & 0 \\ -\nu_{yx}/E_y & 1/E_y & 0 \\ 0 & 0 & 1/G_{xy} \end{bmatrix} \tag{14}$$

The singular strains in the principal directions of the ith lamina are given as

$$\begin{Bmatrix} \varepsilon_1 \\ \varepsilon_2 \\ \gamma_{12} \end{Bmatrix}_i = [T]_i \begin{Bmatrix} \varepsilon_x \\ \varepsilon_y \\ \gamma_{xy} \end{Bmatrix} \tag{15}$$

where the tensor transformation matrix is

$$[T] = \begin{bmatrix} \sin^2\alpha & \cos^2\alpha & \sin 2\alpha \\ \cos^2\alpha & \sin^2\alpha & -\sin 2\alpha \\ -1/2 \sin 2\alpha & 1/2 \sin 2\alpha & -\cos 2\alpha \end{bmatrix} \tag{16}$$

where α is the angle of fiber orientation for the ith lamina and the subscripts 1 and 2 denote directions parallel to the fibers and transverse to the fibers, respectively. (See fig. 7.) Substituting equation (13) into equation (15),

$$\begin{Bmatrix} \varepsilon_1 \\ \varepsilon_2 \\ \gamma_{12} \end{Bmatrix}_i = \frac{K}{E_y\sqrt{2\pi r}} \begin{Bmatrix} \xi_1 \\ \xi_2 \\ \xi_{12} \end{Bmatrix}_i \tag{17}$$

where

$$\begin{Bmatrix} \xi_1 \\ \xi_2 \\ \xi_{12} \end{Bmatrix}_i = [T]_i [\beta] \begin{Bmatrix} \sqrt{E_x E_y} \\ E_y \\ 0 \end{Bmatrix} \tag{18}$$

Note that for $E_x = E_y$, equation (17) becomes

$$\begin{Bmatrix} \varepsilon_1 \\ \varepsilon_2 \\ \gamma_{12} \end{Bmatrix}_i = \frac{(1 - \nu_{yx})K}{E_y\sqrt{2\pi r}} \begin{Bmatrix} 1 \\ 1 \\ 0 \end{Bmatrix}$$

which is independent of α and has the same form for an orthotropic material and an isotropic material.

If we assume that a laminate fails whenever the fiber strains reach a critical level in the principal load-carrying laminae, $\varepsilon_1\sqrt{2\pi r}$ in equation (17) will be a constant at failure. Consequently, $K_Q(\xi_1)_i/E_y$ (where $(\xi_1)_i$ refers to the principal load-carrying laminae) will be a constant at failure independent of laminate orientation. Thus,

$$Q_c = K_Q(\xi_1)_i/E_y \tag{19}$$

is defined as a general fracture-toughness parameter. By substituting equation (11) into equation (19),

$$Q_c = K_{\varepsilon Q}(\xi_1)_i \tag{20}$$

For the 0^o principal load-carrying laminae, equation (18) results in

$$(\xi_1)_i = 1 - \nu_{yx}\sqrt{E_x/E_y} \tag{21}$$

and for both $+45^o$ and -45^o principal load-carrying laminae,

$$(\xi_1)_i = \frac{1}{2}\left(1 - \nu_{yx}\sqrt{E_x/E_y}\right)\left(1 + \sqrt{E_y/E_x}\right) \tag{22}$$

A comparison of equations (21) and (22) shows that axial fiber strains in $\pm 45^{\circ}$ laminae are $1/2\left(1 + \sqrt{E_y/E_x}\right)$ times those in 0° laminae. This factor is 1.08 and 1.05 for the $[0_2/\pm 45]_S$ and $[0/\pm 45]_S$ B/Al laminates, respectively. Thus, one might expect $\pm 45^{\circ}$ fibers to begin breaking before 0° fibers, in contrast to what was generally observed. But an examination of the total elastic strain field (ref. 10) rather than just the singular terms in equation (13) shows that the fiber strains in the $\pm 45^{\circ}$ laminae are greatest for only a very small distance ahead of the slit ends ($r/a < 0.004$). This distance is less than one fiber diameter for the longest slit tested. Therefore, to all intents and purposes the fiber strains are highest in the 0° laminae near the slit ends.

It is interesting to note that the fracture surfaces of specimens with $\pm 45^{\circ}$ laminae gave evidence of very high biaxial strains in the $\pm 45^{\circ}$ fiber directions, like those predicted by equation (17). A portion of the fracture surface of a $[0/\pm 45]_S$ specimen is shown in figure 8. The specimen was photographed with a scanning electron microscope and tilted to enhance the three-dimensional image. Most of the $+45^{\circ}$ and -45° fibers are split as though each failed by cleavage due to transverse strains.

Results and Discussion

Values of the general fracture-toughness parameter Q_c are given in table IV for each laminate orientation. They were calculated three different ways to show the effects of the nonlinear stress-strain behavior of the laminates: (1) With equation (20) and the average $K_{\varepsilon Q}$ values in table III, (2) with equation (19) and the average K_Q values in table III, and (3) same as (2) but with E_{uy} instead of E_y. The values of ξ_1 were calculated with the elastic moduli in table I. (The subscript i has been dropped for brevity.) Equation (22) was used for the $[\pm 45]_{2S}$ laminate orientation and equation (21) was used for the other laminate orientations.

The Q_c values in table IV are plotted in figure 9 for comparison. The $Q_c = \xi_1 K_{\varepsilon Q}$ values are intermediate between the $Q_c = \xi_1 K_Q/E_y$ and $Q_c = \xi_1 K_Q/E_{uy}$ values as expected and generally closer to the latter. For a linear elastic material they should have been equal. But for a nonlinear material like B/Al, the $Q_c = \xi_1 K_Q/E_{uy}$ and the $Q_c = \xi_1 K_Q/E_y$ values give upper and lower bounds, respectively. The actual value of Q_c should be intermediate and probably closer to $Q_c = \xi_1 K_{\varepsilon Q}$. The difference between the upper and lower bounds is small for $[0]_{6T}$ laminates but increases with increasing nonlinearity and, hence, with the proportion of $\pm 45^{\circ}$ laminae.

Except for the $[\pm 45]_{2S}$ laminates, the $Q_c = \xi_1 K_{\varepsilon Q}$ values are approximately equal, as predicted. For $[\pm 45]_{2S}$ laminates, the value is much too high due to the yielding of specimens with small slits, as discussed previously. For $[0]_{6T}$ laminates, the value is close to the others but slightly elevated due to the extensive damage at the ends of long slits. Thus, some of the tests for determining Q_c were not valid. For example, if the values for $[\pm 45]_{2S}$ specimens with slits 5.1 mm and smaller are dropped, the Q_c value in table IV will decrease from 0.02156 $\sqrt{\text{mm}}$ to 0.01396 $\sqrt{\text{mm}}$. Likewise, if the values for $[0]_{6T}$ specimens with slits 15.2 mm and larger are dropped, Q_c will decrease from 0.01328 $\sqrt{\text{mm}}$ to 0.01102 $\sqrt{\text{mm}}$. Then the Q_c values will be reasonably constant

for all the laminate orientations. But they would still increase slightly with the proportion of ±45° laminae, perhaps because of the nonlinear stress-strain behavior.

In order to show how well the general fracture-toughness parameter Q_c would predict strengths of the different laminate orientations, values of strength were predicted with an average value of Q_c and compared with those of the specimens that were tested. First, the values of $Q_c = \xi_1 K_{\epsilon Q}$ in table IV were averaged for $[0_2/\pm45]_S$, $[\pm45/0_2]_S$, and $[0/\pm45]_S$ laminates. Values for $[0]_{6T}$ and $[\pm45]_{2S}$ laminates were not included because they were elevated, as discussed previously. The average value is shown in figure 9 as the dashed line. Second, the average value of Q_c was used to calculate $K_{\epsilon Q}$ and K_Q for each laminate orientation. The procedure was simply the reverse of that used to calculate the Q_c values in table IV. Values of $K_{\epsilon Q}$ were calculated with $K_{\epsilon Q} = Q_c/\xi_1$ and values of K_Q with both $K_Q = Q_c E_y/\xi_1$ and $K_Q = Q_c E_{uy}/\xi_1$. These results are given in table V. Next, strengths and remote failing strains were calculated with equations (5) and (8) and the values of K_Q and $K_{\epsilon Q}$ in table V. And last, values of remote failing strain were converted to strength by using the average stress-strain equations in reference 4. Thus, three values of strength were predicted, two with K_Q and one with $K_{\epsilon Q}$.

The predicted strengths are plotted against slit length for each laminate orientation in figure 10. The strengths were multiplied by the finite-width correction factor $\sqrt{\sec(\pi a/W)}$ to eliminate the effect of specimen width. However, for $[\pm45]_{2S}$ laminates, the predicted values of $S_c\sqrt{\sec(\pi a/W)}$ were still affected by specimen width because F_{tu} and ϵ_{tu} used in equations (5) and (8) were affected by width. (See table I.) However, because of the scale in figure 10, the effect can only be seen in the solid curves. The dashed and dot-dashed curves are affected only for very small slits.

The test strengths in table II were averaged for identical specimens, multiplied by the finite-width correction factor, and plotted in figure 10 for comparison with the predictions. Different symbols are used for different specimen widths. Also, the ultimate tensile strengths in table I are plotted at $a = 0$. The outcome is much like that for the Q_c values in figure 9. The strengths predicted with the $K_{\epsilon Q}$ values agree well with the test values, even generally for the $[0]_{6T}$ and $[\pm45]_{2S}$ specimens. However, as expected, there is some disagreement for $[0]_{6T}$ specimens with large slits and $[\pm45]_{2S}$ specimens with small slits. The strengths predicted with K_Q from E_y and E_{uy} do not agree as well with the test values but rather give upper and lower bounds, respectively. Furthermore the difference between the upper and lower bounds increases with the proportion of ±45° laminae.

As expected, all the laminate orientations with 0° laminae are very notch sensitive; that is, the strengths in figure 10 of specimens with small slits are much smaller than the strengths of specimens without slits. The notch sensitivity of $[\pm45]_{2S}$ specimens is surprisingly large, especially because the failing strains of specimens without slits is so large.

For laminate orientations with ±45° laminae, the test strengths in figure 10 are slightly layered for 50.8-mm- and 101.6-mm-wide specimens. The degree of layering increases with the proportion of ±45° laminae. Therefore,

the finite-width correction factor $\sqrt{\sec(\pi a/W)}$ did not fully account for variations in width. Perhaps the linear elastic correction factor was inaccurate due to the very nonlinear stress-strain behavior of the laminate orientations with $\pm 45^{\circ}$ laminae.

If the stress-intensity factor analysis is valid (e.g., damage is small at the slit ends) and the failure criterion is valid, the general fracture-toughness parameter Q_c should be independent of laminate orientation for other composite materials as well. However, Q_c should vary with the ultimate tensile strain of the fibers ε_{tuf} because the level of fiber strains at the slit ends was assumed to be constant at failure. Indeed, the fracture-toughness data here and that for epoxy composites in table 5 of reference 9 indicate that $Q_c \approx 1.6\varepsilon_{tuf}$. (The quasi-isotropic laminates in table 5 of ref. 9 were made from graphite/epoxy, boron/epoxy, and E-glass/epoxy materials.) From $Q_c = 1.6\varepsilon_{tuf}$ and equations (10) and (20) the damage-zone size can be written as

$$\rho_{\varepsilon c} = \frac{1}{\pi}\left(\frac{1.6\varepsilon_{tuf}}{\xi_1 \varepsilon_{tu}}\right)^2 \tag{23}$$

Because ξ_1 depends upon laminate constants, equation (23) predicts that damage-zone size at failure is not a constant for all laminates. For the fiber-controlled B/Al laminates reported here, $\varepsilon_{tuf} \approx \varepsilon_{tu}$ and equation (23) predicts that $\rho_{\varepsilon c}$ increases slightly with the proportion of $\pm 45^{\circ}$ laminae, from 1.2 mm for $[0]_{6T}$ laminates to 1.5 mm for $[0/\pm 45]_S$ laminates. These values are close to the values in table III that were calculated individually for the various laminate orientations. The increase in $\rho_{\varepsilon c}$ with increased proportion of $\pm 45^{\circ}$ laminae (according to eq. (23)) is consistent with the trend of the data in table III and figure 6, though the increase is subtle.

For the epoxy laminates in reference 9, $\varepsilon_{tuf} \approx \varepsilon_{tu}$ and ξ_1 varies from about 0.5 for $[0/\pm 45]_S$ laminates to 1.0 for $[0/90]_S$ laminates. Accordingly, equation (23) predicts that $\rho_{\varepsilon c}$ varies from 3.3 to 0.8 mm. The calculated values for damage-zone size in reference 9 are mostly within this range. But they are rather erratic and do not show a clear relationship with laminate orientation such as that given by equation (23).

Fracture toughness was also predicted in reference 9 for the various materials and laminate orientations with $K_Q/F_{tu} = 2.5\sqrt{mm}$. This equation was derived by assuming that damage-zone size at failure was a constant equal to 2.0 mm. (Eq. (4) gives the same result for $\rho_c = 2.0$ mm.) But, from equations (10), (11), and (23) and by assuming $\varepsilon_{tuf} = \varepsilon_{tu}$ and $Q_c = 1.6\varepsilon_{tuf}$, the generalized fracture-toughness parameter predicts

$$K_Q = 1.6F_{tu}/\xi_1 \tag{24}$$

For the quasi-isotropic laminates in reference 9, equation (24) gives $K_Q/F_{tu} = 2.4\sqrt{mm}$, which agrees closely with the equation in reference 9. But for the other laminates in reference 9, equation (24) predicts K_Q/F_{tu} between $1.6\sqrt{mm}$ for symmetrical $[0/90]$ laminates and $3.2\sqrt{mm}$ for symmetrical $[0/\pm45]$ laminates. Equations (23) and (24) only necessarily apply to those laminates for which actual damage to the fibers and matrix at the slit ends is small compared with the slit length. Actual damage was not reported in reference 9, so the validity of these predictions for the different laminates is unknown.

CONCLUDING REMARKS

The fracture toughness of boron/aluminum composites was measured on sheet specimens with central slits that represented cracks. The specimens were axially loaded and had various widths and slit lengths. The sheets were made with five different laminate orientations: $[0]_{6T}$, $[0_2/\pm45]_S$, $[\pm45/0_2]_S$, $[0/\pm45]_S$, and $[\pm45]_{2S}$. Most tests were duplicated.

All laminate orientations were severely weakened by the slits, even $[\pm45]_{2S}$ laminates. Failures of all the specimens were generally collinear with the slit, that is, self-similar. However, the $[0]_{6T}$ specimens gave evidence of a long, narrow region of matrix damage at each end of the slit. There was no evidence of such extensive matrix damage in laminates with $\pm45^o$ laminae. Radiographs show that specimens of all the laminate orientations began failing at the slit ends with what appeared to be tensile failures of fibers in principal load-carrying laminae.

Critical values of both the stress-intensity and strain-intensity factors were calculated for each test using strength and remote failing strain, respectively. Average values were calculated for each laminate orientation. The ratios of stress-to-strain-intensity factors were not proportional to Young's moduli due to the nonlinear stress-strain behavior of the laminates. Values of damage-zone size at the slit ends were also calculated for each laminate orientation. These values, which were about 1.0 to 2.0 mm, agreed with the extent of broken fibers as measured from the radiographs.

A general fracture-toughness parameter Q_c, which is independent of laminate orientation, was derived. Fibers in the principal load-carrying laminae were assumed to fail whenever fiber strains ahead of the slit ends reached a critical level. The resultant parameter Q_c was proportional to the critical value of stress-intensity factor, which was used to describe the strain field ahead of the slit ends. The constant of proportionality depended only on the elastic constants of the laminates.

Values of Q_c were calculated for each B/Al laminate orientation using the average values of the critical stress-intensity and strain-intensity factors. Calculations with the strain-intensity factor gave the best results. Calculations with the stress-intensity factors using ultimate secant and elastic moduli gave upper and lower bounds on Q_c, respectively. Except for $[\pm45]_{2S}$ laminates, Q_c was approximately equal for all the laminate orientations. The value of Q_c for $[\pm45]_{2S}$ laminates was much too large due to the very large remote failing strains of specimens with small slits. Also, the value of Q_c for $[0]_{6T}$

laminates was slightly elevated due to extensive matrix damage at the ends of large slits. Thus, tests of $[0]_{6T}$ specimens with large slits and $[\pm 45]_{2S}$ specimens with small slits were not valid for determining Q_c. In fact, if these values were omitted, Q_c would have been reasonably equal for all the laminate orientations. Likewise, strengths were predicted quite well for all the specimens using an average value of Q_c, again except for $[0]_{6T}$ and $[\pm 45]_{2S}$ specimens with large and small slits, respectively.

The general fracture-toughness parameter Q_c should be independent of laminate orientation for other composite materials as long as the stress-intensity analysis is valid. But Q_c should not be the same constant for all composite materials. In fact, data for several other materials suggested that Q_c is proportional to the ultimate tensile strain of the fibers. It was shown that the fracture toughness could then be predicted from the unnotched tensile strength of the laminate. The size of the damage zone at the slit ends was also shown to vary with the elastic constants of the laminate.

Langley Research Center
National Aeronautics and Space Administration
Hampton, VA 23665
August 26, 1980

REFERENCES

1. Cruse, Thomas A.: Tensile Strength of Notched Composites. J. Compos. Mater., vol. 7, Apr. 1973, pp. 218-229.

2. Konish, H. J., Jr.; Cruse, T. A.; and Swedlow, J. L.: Method for Estimating Fracture Strength of Specially Orthotropic Composite Laminates. Analysis of the Test Methods for High Modulus Fibers and Composites, ASTM, Spec. Tech. Publ. 521, 1973, pp. 133-142.

3. Waszczak, J. P.: On the Applicability of Linear Elastic Fracture Mechanics to 5.6-Mil Boron/6061 Aluminum. AIAA Paper No. 75-786, May 1975.

4. Sova, J. A.; and Poe, C. C., Jr.: Tensile Stress-Strain Behavior of Boron/Aluminum Laminates. NASA TP-1117, 1978.

5. Zweben, Carl: An Approximate Method of Analysis for Notched Unidirectional Composites. Eng. Fract. Mech., vol. 6, no. 1, Mar. 1974, pp. 1-10.

6. Tirosh, J.: The Effect of Plasticity and Crack Blunting on the Stress Distribution in Orthotropic Composite Materials. Trans. ASME, Ser. E: J. Appl. Mech., vol. 40, no. 3, Sept. 1973, pp. 785-790.

7. Paris, Paul C.; and Sih, George C.: Stress Analysis of Cracks. Fracture Toughness Testing and Its Applications, Spec. Tech. Publ. No. 381, American Soc. Testing & Mater., c.1965, pp. 30-85.

8. Chu, C. S.; Anderson, J. M.; Batdorf, W. J.; and Aberson, J. A.: Finite Element Computer Program To Analyze Cracked Orthotropic Sheets. NASA CR-2698, 1976.

9. Caprino, G.; Halpin, J. C.; and Nicolais, L.: Fracture Mechanics in Composite Materials. Composites, vol. 10, no. 4, Oct. 1979, pp. 223-227.

10. Ang, D. D.; and Williams, M. L.: Combined Stresses in an Orthotropic Plate Having a Finite Crack. Trans. ASME, Ser. E: J. Appl. Mech., vol. 28, no. 3, Sept. 1961, pp. 372-378.

TABLE I.- TENSILE PROPERTIES OF B/Al LAMINATES WITHOUT SLITS

Laminate orientation	W, mm	F_{tu}, MPa	ε_{tu}	ν_{yx}	E_x, GPa	E_y, GPa	$^aE_{uy}$, GPa
$[0]_{6T}$	19.1	1672.0	0.007908	0.2049	143.1	237.3	211.40
$[0_2/\pm45]_S$	19.1	800.1	.007267	.2513	130.1	176.2	110.10
$[\pm45/0_2]_S$	19.1	910.5	.008205	.2519	134.7	177.5	111.00
$[0/\pm45]_S$	19.1	581.4	.007008	.2911	129.5	159.2	83.00
$[\pm45]_{2S}$	19.1	220.6	^{b}.049710	.3247	126.2	126.9	4.44
$[\pm45]_{2S}$	50.8	280.8	^{b}.063040	------	-----	-----	4.45
$[\pm45]_{2S}$	101.6	330.9	^{b}.069190	------	-----	-----	4.78

$^aE_{uy} = F_{tu}/\varepsilon_{tu}$.
^{b}Calculated from residual change in specimen width.

TABLE II.- FRACTURE DATA

(a) $[0]_{6T}$ laminates

W, mm	2a, mm	S_c, MPa	K_Q, MPa$\sqrt{m}$	ε_{oc}		$K_{\varepsilon Q}$, $\sqrt{m}$
				Measured	Calculated (a)	(b)
19.1	[c]0.5	1365	2097	0.00648	0.00667	0.01003
	[c].5	1371	2125	.00657	.00670	.01048
	[c]1.3	1124	2181	.00573	.00542	.01195
	[c]1.3	1165	2334	.00554	.00563	.01116
50.8	[c]2.5	929	2219	0.00412	0.00443	0.00958
	[c]2.5	1051	2685	.00492	.00505	.01248
	5.1	921	3152	.00412	.00439	.01378
	5.1	934	3216	.00422	.00445	.01425
	15.2	665	3794	.00275	.00311	.01770
	15.2	666	3801	.00263	.00312	.01777
	[d]15.2	701	4049	.00252	.00329	.01897
	[d]15.2	645	3657	.00251	.00301	.01702
	25.4	534	4336	.00172	.00247	.01998
	25.4	502	4037	.00164	.00232	.01860
101.6	[c]5.1	969	3373	0.00471	0.00463	0.01664
	10.2	790	3617	.00373	.00373	.01707
	10.2	775	3529	.00366	.00366	.01666
	30.5	541	4223	.00202	.00251	.01955
	30.5	506	3918	.00193	.00234	.01807
	[d]30.5	470	3611	.00172	.00216	.01655
	50.8	393	4348	.00110	.00180	.01986
	50.8	382	4217	.00115	.00174	.01915

[a]Calculated with Ramberg-Osgood equation (ref. 4).
[b]Calculated values of ε_{oc} were used for $2a \geq 15.2$ mm.
[c]Crack-opening displacement (COD) bracket used.
[d]Specimen radiographed.

TABLE II.- Continued

(b) $[0_2/\pm45]_S$ laminates

W, mm	2a, mm	S_c, MPa	K_Q, MPa $\sqrt{m}$	ε_{oc}	$K_{\varepsilon Q}$, $\sqrt{m}$
19.1	[a]0.5	703	1307	0.00647	0.01262
	[a]1.3	628	1459	.00560	.01265
	[a]1.3	624	1435	.00553	.01226
50.8	[a]2.5	569	1609	0.00475	0.01247
	[a]2.5	585	1705	.00499	.01364
	5.1	463	1622	.00398	.01358
	5.1	451	1560	.00381	.01277
	15.2	309	1752	.00244	.01351
	15.2	325	1863	.00255	.01421
	[b]15.2	317	1807	.00249	.01383
	[b]15.2	314	1787	.00244	.01351
	25.4	219	1740	.00167	.01304
	25.4	220	1749	.00161	.01254
101.6	[a,c]5.1	447	1529	0.00413	0.01424
	[a,c]5.1	479	1697	.00472	.01762
	[a]10.2	389	1797	.00321	.01443
	[a]10.2	354	1592	.00287	.01260
	[a]30.5	259	2022	.00195	.01492
	[b]30.5	254	1978	.00189	.01442
	[a]50.8	177	1948	.00121	.01311
	[a]50.8	189	2092	.00130	.01413

[a]COD bracket used.
[b]Specimen radiographed.
[c]Specimen 355 mm long.

TABLE II.- Continued

(c) $[\pm 45/0_2]_S$ laminates

W, mm	2a, mm	S_c, MPa	K_Q, MPa$\sqrt{m}$	ε_{oc}	$K_{\varepsilon Q}$, $\sqrt{m}$
50.8	[a]2.5	575	1473	0.00488	0.01206
	[a]2.5	552	1379	.00471	.01142
	5.1	483	1627	.00415	.01373
	5.1	484	1632	.00410	.01351
	15.2	332	1863	.00266	.01466
	15.2	327	1830	.00264	.01453
	[b]15.2	333	1869	[c].00258	.01416
	[b]15.2	324	1810	.00263	.01447
	25.4	229	1803	.00173	.01342
	25.4	218	1708	.00166	.01285
101.6	[a]5.1	461	1516	0.00388	0.01249
	[a]5.1	500	1697	.00446	.01507
	[a]10.2	388	1730	.00325	.01427
	[a]10.2	382	1697	.00320	.01401
	[a]30.5	254	1950	.00190	.01437
	[a]30.5	257	1975	.00200	.01518
	[a]50.8	178	1944	.00127	.01373
	[a]50.8	188	2060	.00131	.01417

[a]COD bracket used.
[b]Specimen radiographed.
[c]Calculated with Ramberg-Osgood equation (ref. 4).

TABLE II.- Continued

(d) $[0/\pm45]_S$ laminates

W, mm	2a, mm	S_c, MPa	K_Q, MPa$\sqrt{m}$	ε_{oc}	$K_{\varepsilon Q}$, $\sqrt{m}$
19.1	[a]1.3	480	1227	0.00575	0.01450
	[a]1.3	483	1252	.00576	.01458
50.8	[a]2.5	433	1290	0.00467	0.01245
	[a]2.5	493	1853	.00561	.01863
	5.1	426	1796	.00497	.02021
	5.1	423	1769	.00496	.02012
	15.2	269	1597	.00283	.01620
	15.2	250	1453	.00265	.01497
	[b]15.2	286	1734	.00289	.01662
	[b]15.2	261	1535	.00257	.01443
	25.4	195	1597	.00179	.01411
	25.4	188	1530	.00174	.01368
101.6	[a,c]5.1	406	1610	0.00496	0.01993
	[a,c]5.1	394	1521	.00464	.01757
	10.2	368	1923	.00417	.02097
	10.2	353	1796	[d].00372	.01772
	30.5	235	1907	.00239	.01880
	30.5	250	2059	.00271	.02179
	[b]30.5	236	1917	.00221	.01719
	50.8	149	1662	.00135	.01473
	50.8	166	1875	.00159	.01754

[a]COD bracket used.
[b]Specimen radiographed.
[c]Specimen 355 mm long.
[d]Calculated with Ramberg-Osgood equation (ref. 4).

TABLE II.- Concluded

(e) $[\pm 45]_{2S}$ laminates

W, mm	2a, mm	S_c, MPa	K_Q, MPa$\sqrt{\text{mm}}$	ε_{oc}	$K_{\varepsilon Q}$, mm
19.1	[a]0.5	189.0	325	[b]0.02482	0.02540
	[a]1.3	164.0	353	[b].01330	.01979
	[a]1.3	165.0	358	[b].01365	.02035
50.8	[a]2.5	232.0	820	0.03500	0.08357
	[a]2.5	252.0	1141	.03747	.09255
	5.1	170.0	611	.02079	.06277
	5.1	162.0	567	.01838	.05476
	15.2	108.0	612	.00413	.02142
	15.2	107.0	605	.00397	.02059
	[c]15.2	131.0	780	.00311	.01612
	[c]25.4	94.3	773	.00165	.01240
	25.4	73.6	582	.00128	.00962
	25.4	73.2	578	.00143	.01075
101.6	[a,d]5.1	129.0	397	0.01685	0.04925
	[a,d]5.1	182.0	618	.00842	.02405
	10.2	135.0	596	.00800	.03244
	10.2	138.0	612	.01176	.04808
	30.5	98.1	758	.00275	.02018
	30.5	98.7	763	.00315	.02313
	[c]30.5	126.0	1010	.00298	.02188
	50.8	70.5	774	.00143	.01520
	50.8	72.7	800	.00152	.01615

[a]COD bracket used.
[b]Calculated with Ramberg-Osgood equation (ref. 4).
[c]Specimen radiographed.
[d]Specimen 355 mm long.

TABLE III.- MEASURED FRACTURE TOUGHNESSES AND CORRESPONDING DAMAGE-ZONE SIZES

Laminate orientation	K_Q, MPa$\sqrt{mm}$		$K_{\varepsilon Q}$, $\sqrt{mm}$		ρ_c, mm	$\rho_{\varepsilon c}$, mm
	Average	Coefficient of variation	Average	Coefficient of variation		
$[0]_{6T}$	3387	0.229	0.01579	0.218	1.31	1.27
$[0_2/\pm45]_S$	1717	.117	.01362	.088	1.47	1.12
$[\pm45/0_2]_S$	1754	.076	.01378	.074	1.18	.90
$[0/\pm45]_S$	1662	.140	.01699	.158	2.60	1.87
$[\pm45]_{2S}$	656	.309	.03184	.733	[a]2.81 to 1.25	[a]0.13 to 0.07

[a]For specimen widths from 19.1 to 101.6 mm.

TABLE IV.- GENERAL FRACTURE-TOUGHNESS

PARAMETER Q_c

Laminate orientation	ξ_1	Q_c, $\sqrt{mm}$, calculated from -		
		$\xi_1 K_{\varepsilon Q}$	$\xi_1 K_Q/E_y$	$\xi_1 K_Q/E_{uy}$
$[0]_{6T}$	0.8409	0.01328	0.01200	0.01347
$[0_2/\pm45]_S$	.7841	.01068	.00764	.01223
$[\pm45/0_2]_S$	.7806	.01074	.00771	.01233
$[0/\pm45]_S$	.7375	.01250	.00770	.01477
$[\pm45]_{2S}$	.6771	.02156	.00350	.1001

TABLE V.- PREDICTED FRACTURE TOUGHNESSES

$[Q_c = 0.01131\ \sqrt{mm}]$

Laminate orientation	$^aK_{\varepsilon Q}$, $\sqrt{mm}$	K_Q, MPa$\sqrt{mm}$, calculated from -	
		$Q_c E_y/\xi_1$	$Q_c E_{uy}/\xi_1$
$[0]_{6T}$	0.01345	3191	2843
$[0_2/\pm45]_S$	.01442	2541	1588
$[\pm45/0_2]_S$	.01449	2571	1608
$[0/\pm45]_S$	.01533	2441	1278
$[\pm45]_{2S}$	.01670	2119	^{b}74

$^aK_{\varepsilon Q} = Q_c/\xi_1$.
$^bE_{uy}$ = 4.44 GPa was used for all widths.

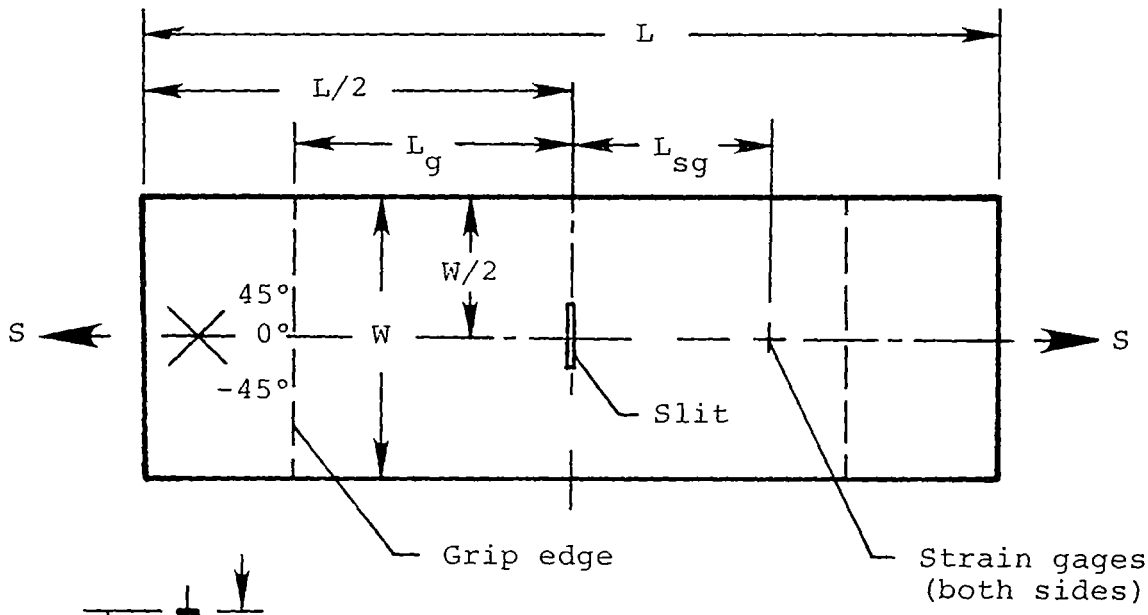

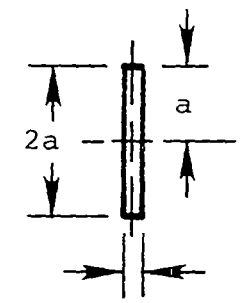

0.18-0.25 mm

Slit Detail

W, mm	L, mm	L_g, mm	L_{sg}, mm
19.1	254	75	38
50.8	254	80	64
101.6	475	150	89
101.6	355	100	89

Figure 1.- Specimen configuration.

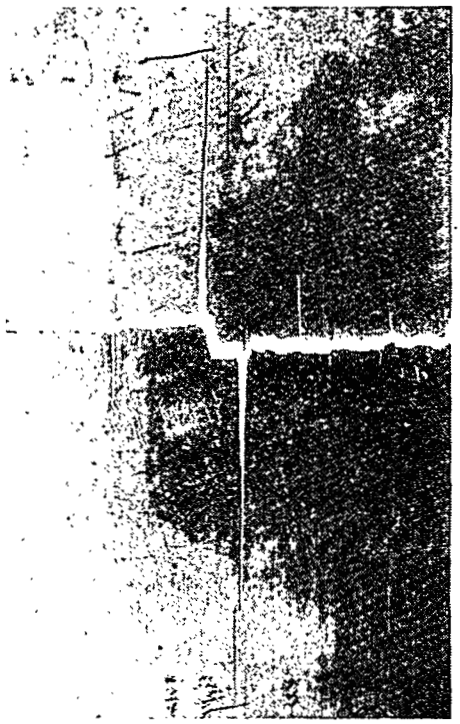

2a = 5.1 mm

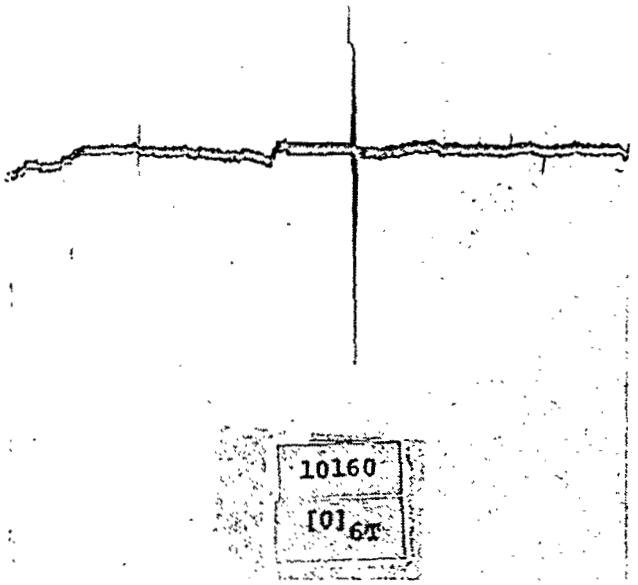

2a = 10.2 mm

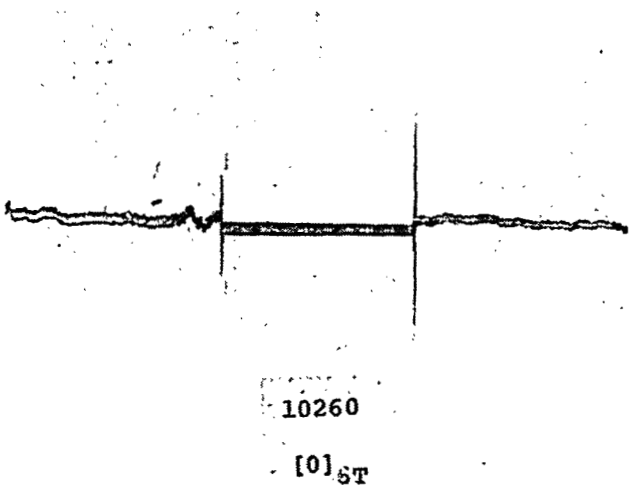

2a = 30.5 mm

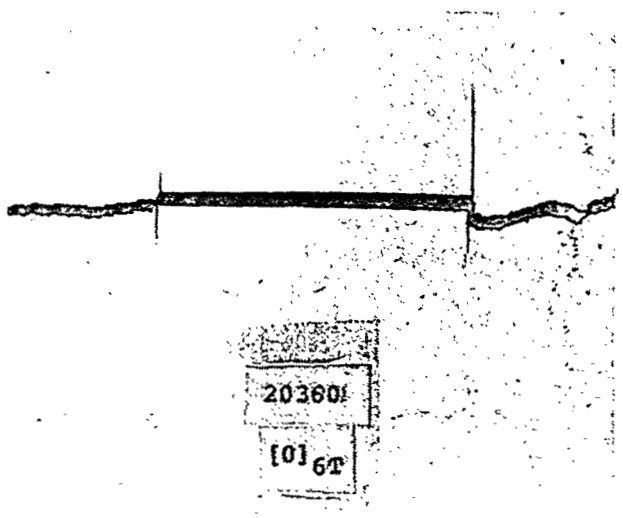

2a = 50.8 mm

L-80-188

Figure 2.- Photographs of failed 101.6-mm-wide $[0]_{6T}$ specimens.

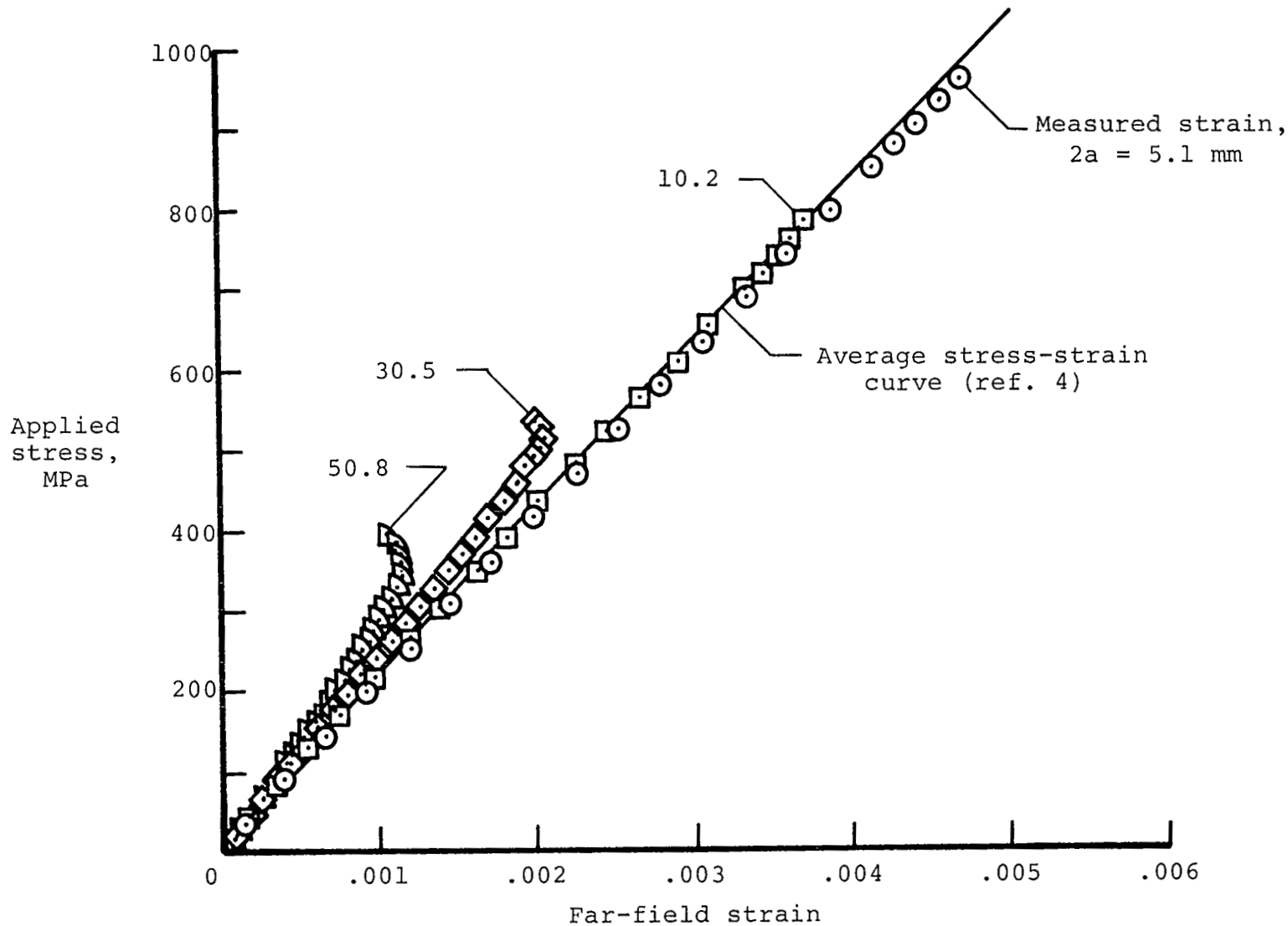

Figure 3.- Effect of matrix damage on far-field strain for 101.6-mm-wide $[0]_{6T}$ specimens with several slit lengths.

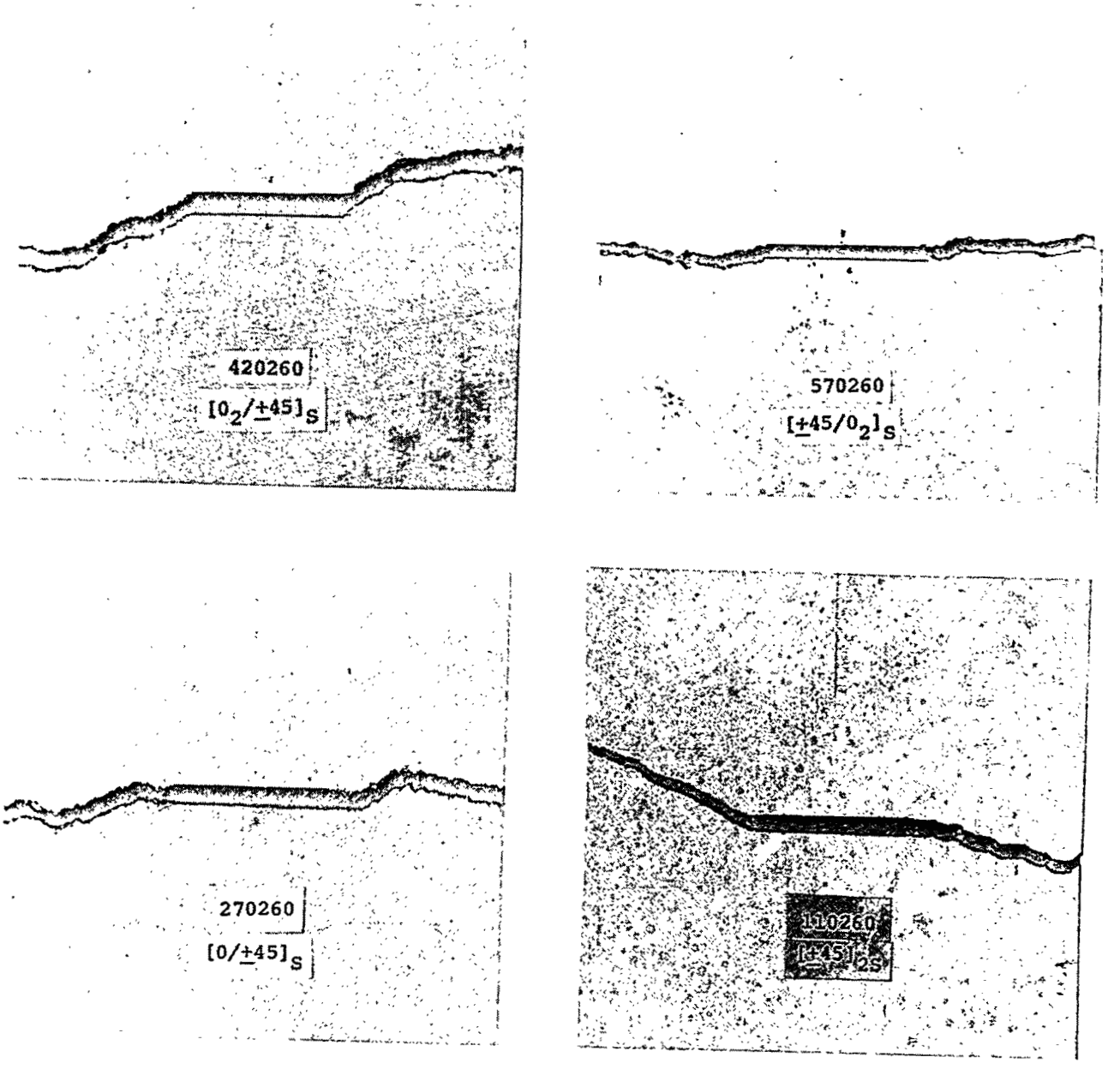

L-80-189

Figure 4.- Photographs of failed 101.6-mm-wide specimens with various proportions of $\pm45^{\circ}$ laminae. 2a = 30.5 mm.

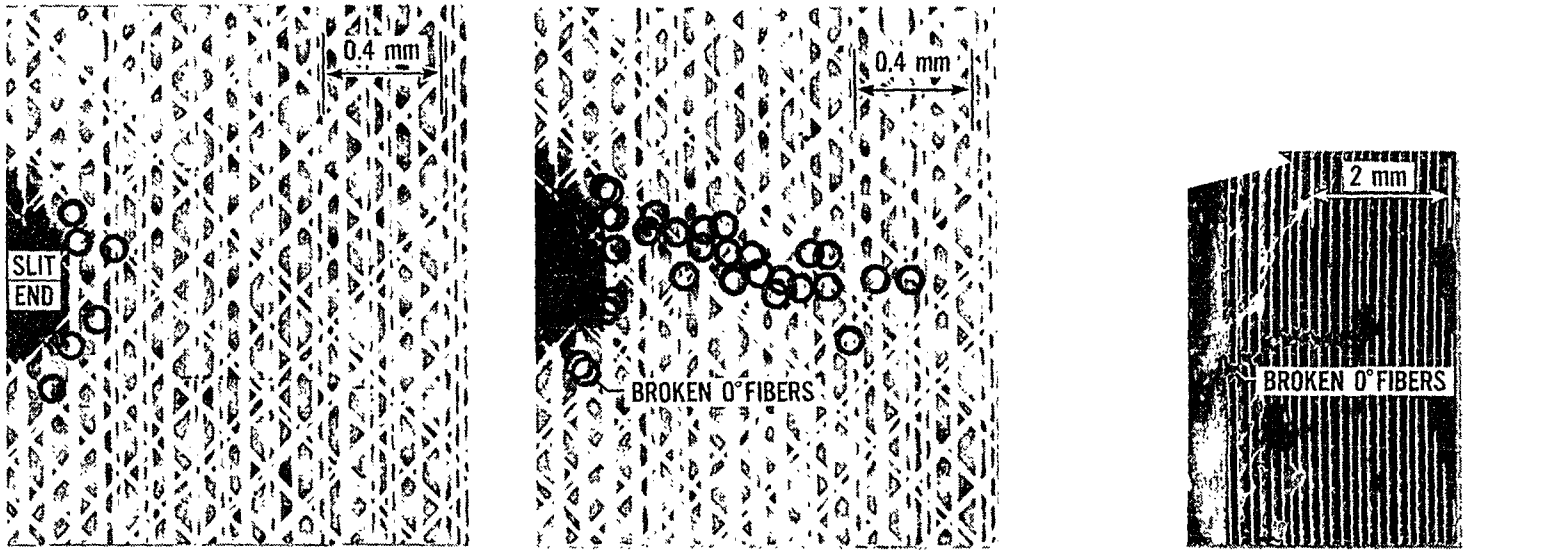

L-80-190

Figure 5.- Broken 0^{o} fibers in $[\pm 45/0_2]_s$ laminates. 2a/W = 0.3.

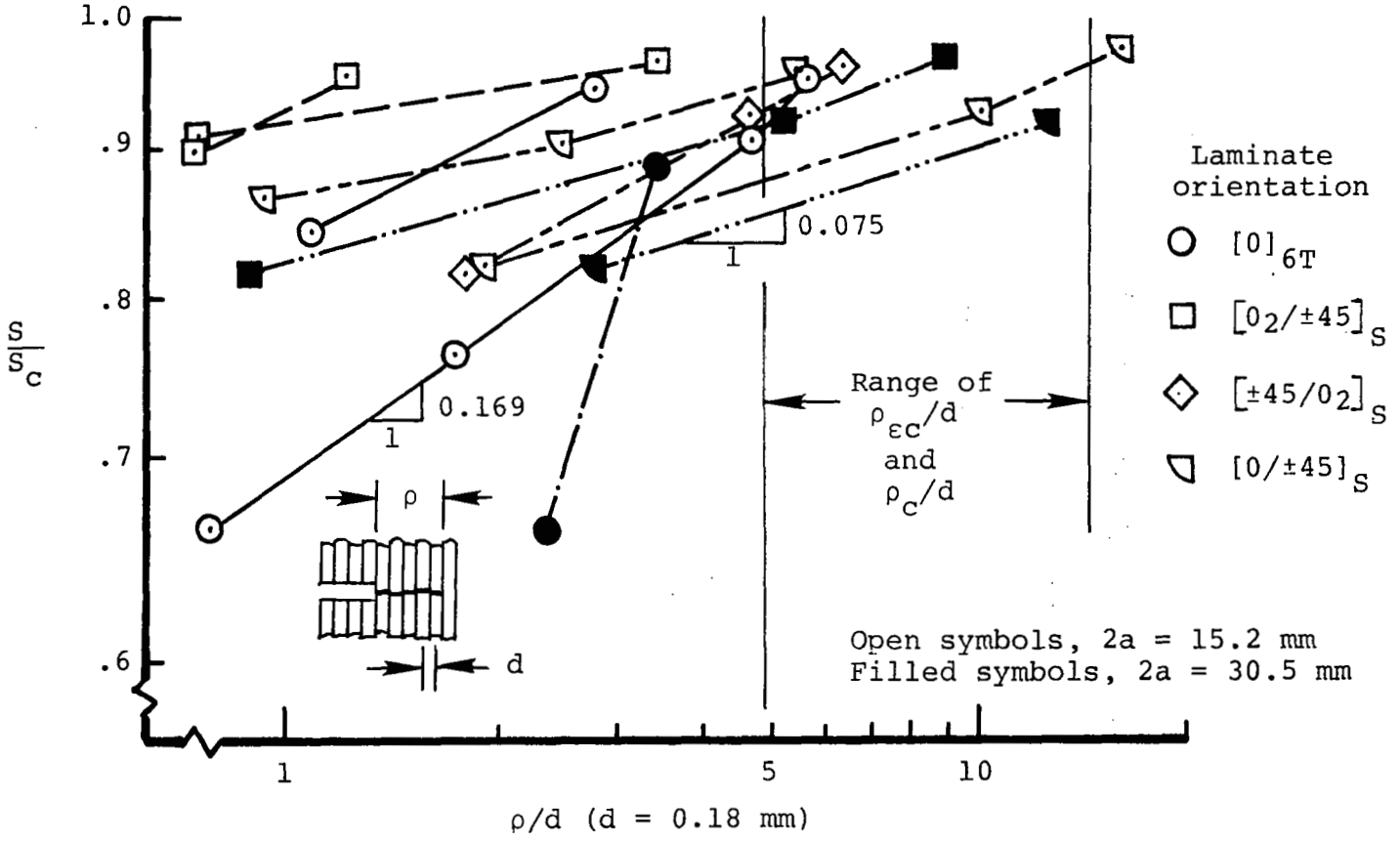

Figure 6.- Extent of broken 0° fibers in radiographs. 2a/W = 0.3.

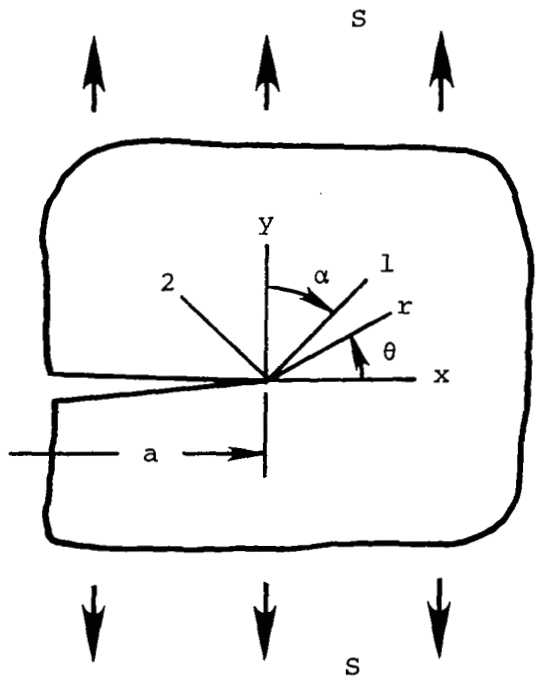

Figure 7.- Laminate and principal lamina coordinates.

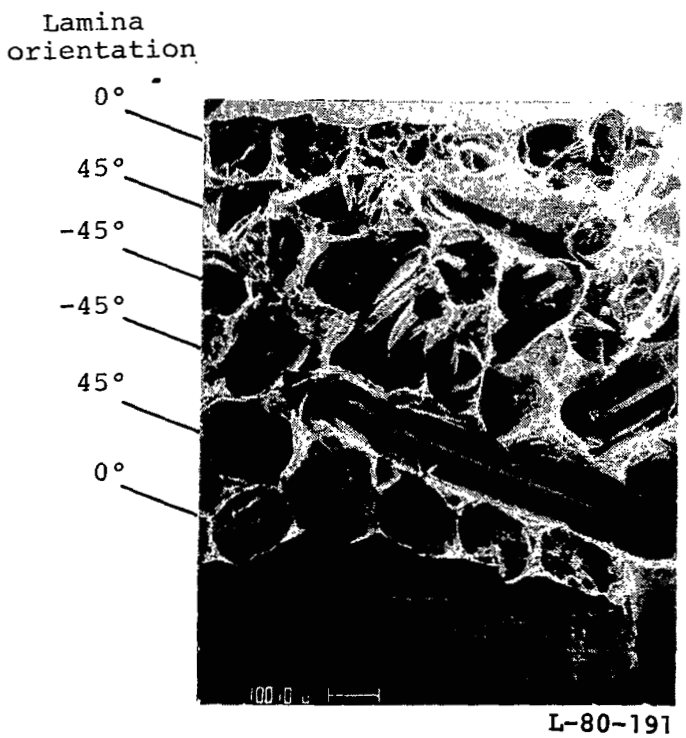

Figure 8.- Fracture surface of $[0/\pm45]_S$ specimen (×70). Specimen is tilted up.

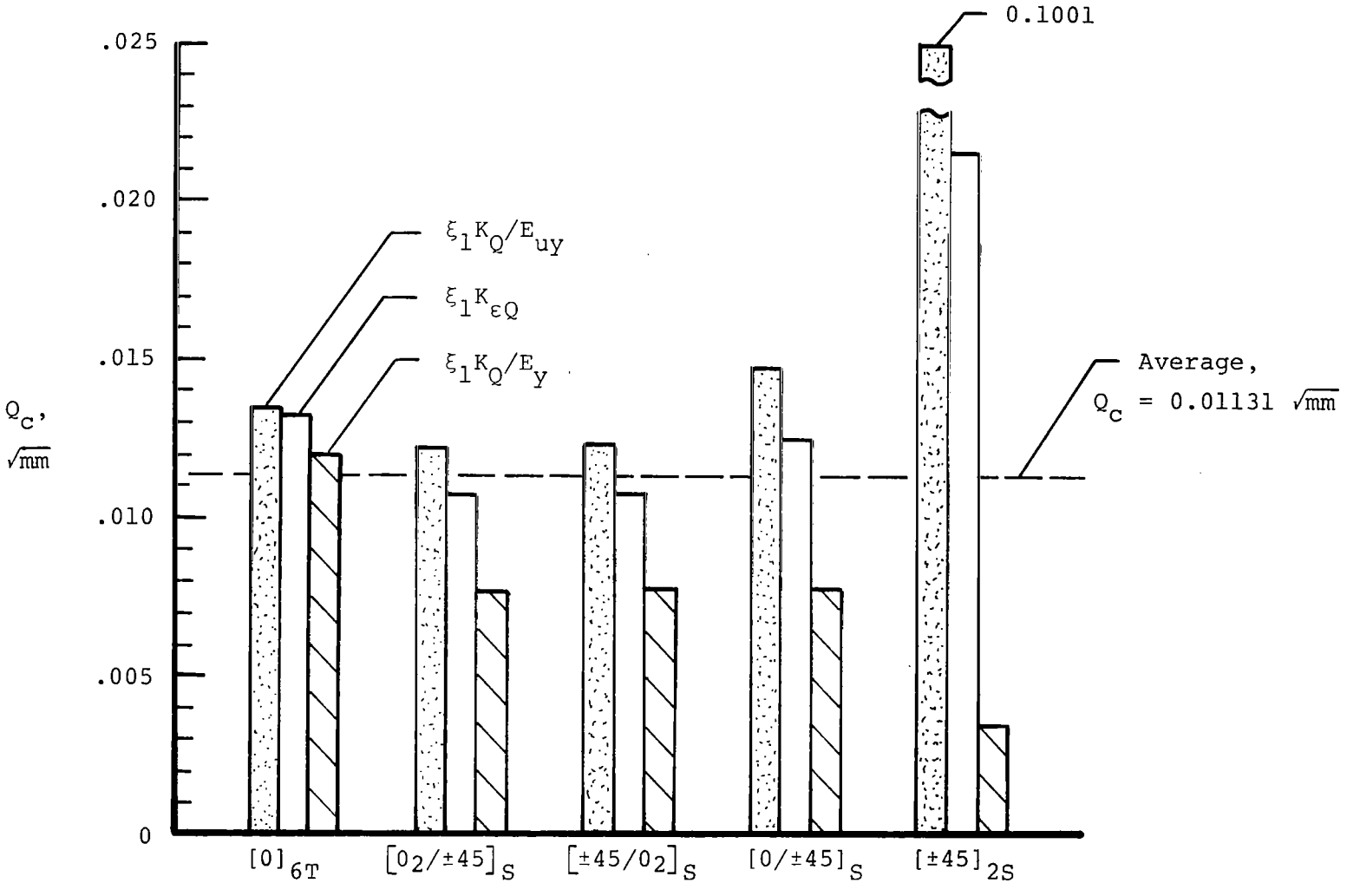

Figure 9.- Values of the general fracture-toughness parameter.

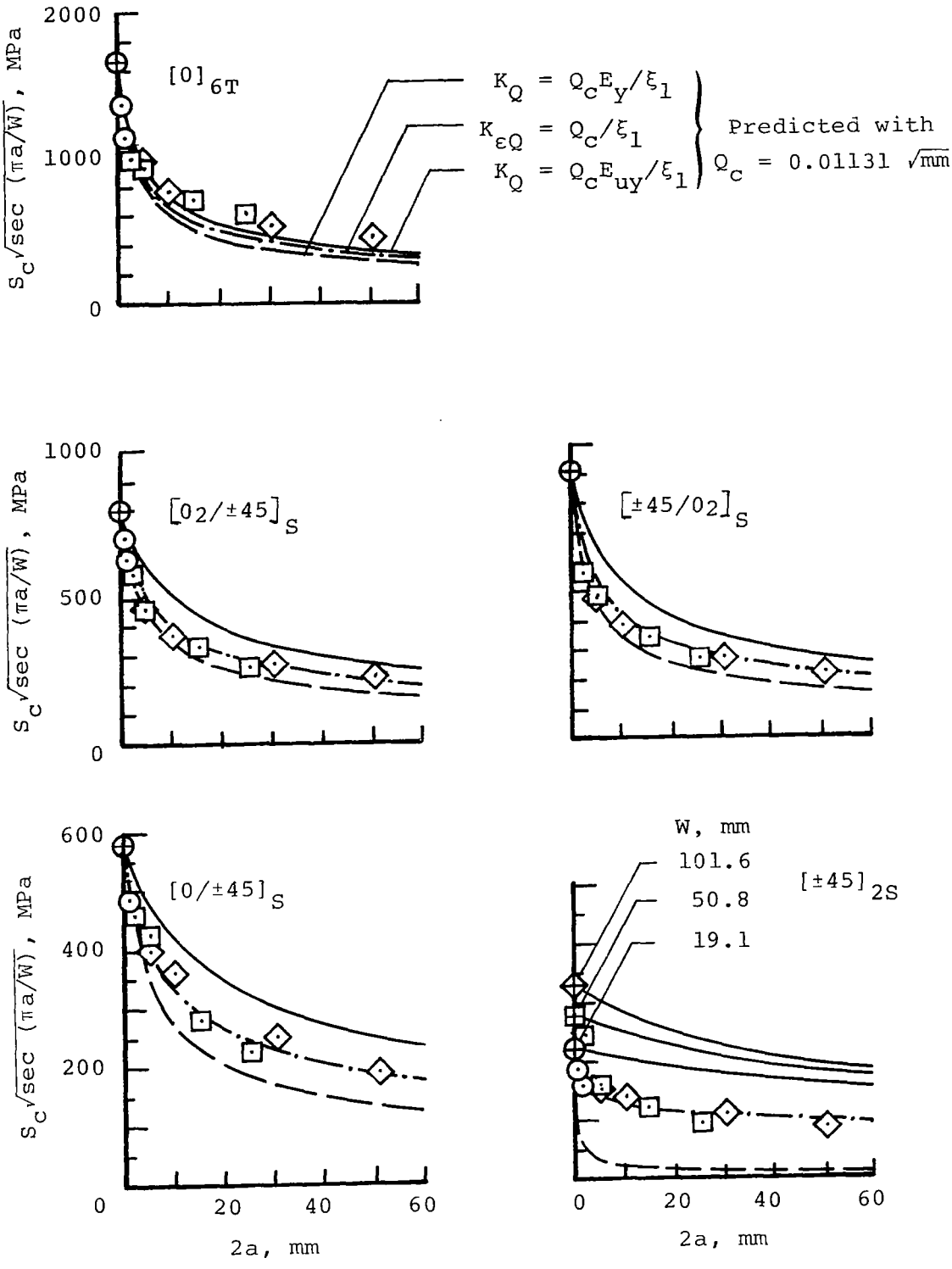

Figure 10.- Measured and predicted strengths. ("+" inside symbols indicates F_{tu} in table I.)

1. Report No. NASA TP-1707	2. Government Accession No.	3. Recipient's Catalog No.
4. Title and Subtitle FRACTURE TOUGHNESS OF BORON/ALUMINUM LAMINATES WITH VARIOUS PROPORTIONS OF 0° AND ±45° PLIES		5. Report Date November 1980 6. Performing Organization Code
7. Author(s) C. C. Poe, Jr., and J. A. Sova		8. Performing Organization Report No. L-13880 10. Work Unit No. 533-01-13-02
9. Performing Organization Name and Address NASA Langley Research Center Hampton, VA 23665		11. Contract or Grant No.
12. Sponsoring Agency Name and Address National Aeronautics and Space Administration Washington, DC 20546		13. Type of Report and Period Covered Technical Paper 14. Sponsoring Agency Code

15. Supplementary Notes

C. C. Poe, Jr.: Langley Research Center.

J. A. Sova: The George Washington University, Joint Institute for Advancement of Flight Sciences, Langley Research Center, Hampton, Virginia.

16. Abstract

The fracture toughness of boron/aluminum laminates was measured on sheet specimens containing central slits of various lengths that represented cracks. The specimens were loaded axially and had various widths. The sheets were made with five laminate orientations: $[0]_{6T}$, $[0_2/\pm45]_S$, $[\pm45/0_2]_S$, $[0/\pm45]_S$, and $[\pm45]_{2S}$. Fracture toughness was calculated for each laminate orientation. Specimens began failing at the ends of the slit with what appeared to be tensile failures of fibers in the primary load-carrying laminae.

A general fracture-toughness parameter independent of laminate orientation was derived on the basis of fiber failure in the principal load-carrying laminae. The value of this parameter was proportional to the critical value of the stress-intensity factor. The constant of proportionality depended only on the elastic constants of the laminates. The values of the fracture-toughness parameter were about equal except for $[0]_{6T}$ specimens with long slits and $[\pm45]_{2S}$ specimens with small slits. Those specimens had too much matrix damage and gross yielding, respectively. The parameter was also shown to be proportional to the ultimate tensile strain of the fibers. The fracture toughness could then be predicted solely from the ultimate tensile strength of the laminate.

17. Key Words (Suggested by Author(s))	18. Distribution Statement
Boron/aluminum Fracture toughness Cracked-strength prediction	Unclassified - Unlimited Subject Category 24

19. Security Classif. (of this report)	20. Security Classif. (of this page)	21. No. of Pages	22. Price
Unclassified	Unclassified	36	A03

For sale by the National Technical Information Service, Springfield, Virginia 22161

NASA-Langley, 1980

7 1 1U,C, 101580 S00903DS
DEPT OF THE AIR FORCE
AF WEAPONS LABORATORY
ATTN: TECHNICAL LIBRARY (SUL)
KIRTLAND AFB NM 87117